Spin Crossover in Ferropericlase from First-Principles Molecular Dynamics

E. Holmström* and L. Stixrude
Department of Earth Sciences, University College London, Gower Street, London WC1E 6BT, United Kingdom
(Received 20 November 2014; published 19 March 2015)

Ferropericlase, (Mg,Fe)O, is the second-most abundant mineral of Earth's lower mantle. With increasing pressure, the Fe ions in the material begin to collapse from a magnetic to nonmagnetic spin state. We present a finite-temperature first-principles phase diagram of this spin crossover, finding a broad pressure range with coexisting magnetic and nonmagnetic ions due to favorable enthalpy of mixing of the two. Furthermore, we find the electrical conductivity of the mineral to reach semimetallic values inside Earth.

DOI: 10.1103/PhysRevLett.114.117202 PACS numbers: 75.30.Wx, 91.60.Gf, 91.60.Pn

Ferropericlase, $(Mg_{1-x}Fe_x)O$, is an Fe-bearing transition-metal oxide that makes up some 20% of the total volume of Earth's lower mantle [1]. Each Fe ion in this mineral assumes an octahedral coordination environment, which leads to crystal field splitting, i.e., separation of the Fe $3d$ shell of electrons into a higher-energy e_g and a lower-energy t_{2g} group. At low pressure, the ground-state electronic configuration of Fe^{2+} is a high-spin state with four unpaired electrons giving a total spin of $S = 2$. On compression, three effects come into play that ultimately cause a spin transition or magnetic collapse to the low-spin state, $S = 0$. First, the crystal field splitting grows due to increased overlap of the Fe and O valence orbitals, while second, the electronic bands are broadened in energy due to increased confinement, making the high-spin state increasingly unfavorable [2,3]. Third, the low-spin state is favored by the smaller size of the low-spin Fe ion via the $P\Delta V$ contribution to the free energy [4,5].

Ever since the discovery of the spin transition in $Fe_{0.94}O$ beyond 60 GPa at room temperature [6] and later in ferropericlase between pressures of 50 to 70 GPa [7], it has become apparent that the phenomenon affects mechanical [5,8–11], compositional [7], and electronic properties [12,13] and, thus, holds potentially significant implications for the physics and chemistry of Earth. Interest in spin transitions is not, however, limited to geoscience, with applications in, e.g., nanoclusters and thin films showing great technological potential [14]. Experimental work utilizing x-ray emission spectroscopy (XES) [7,8], optical spectroscopy [12], Mössbauer spectroscopy (MSB) [15], and equation-of-state (EOS) data gathered from high-pressure x-ray diffraction experiments [16] has, to date, probed the spin transition in ferropericlase up to pressures of $P = 140$ GPa and temperatures of $T = 2000$ K. On the theoretical side, approaches based on analytical mean-field theory [17] and static first-principles calculations [18] augmented by quasiharmonic phonon computations [10] have treated the spin transition as in fact a smooth *spin crossover*, an approach consistent with published experiments. This crossover proceeds, with increasing pressure, from all Fe ions assuming the high-spin state, through to a mixed-spin phase with coexisting high-spin and low-spin ions, to eventually all ions assuming the low-spin state.

Previous theoretical work has been based on static calculations and has assumed that the mixed-spin state is stabilized entropically, yielding a narrow crossover at low temperatures that disagrees with experiment. Moreover, experiment and theory have not explored geophysically important properties such as the band structure and electrical conductivity. In this Letter, we take a different approach that combines first-principles molecular dynamics with free-energy minimization to simulate the high-temperature properties of the spin crossover directly. Our results reveal a new physical picture of the crossover, where the mixed-spin phase is stabilized through enthalpy rather than entropy, giving a finite broadness for the crossover even at vanishing temperatures. Additionally, we predict the EOS up to the conditions at the base of Earth's mantle (140 GPa, 4000 K) and find that the electrical conductivity of ferropericlase reaches semimetallic values at the bottom of the lower mantle, with significant geophysical implications.

Our simulation setup is built on molecular dynamics (MD) simulations within density functional theory (DFT), as implemented in the VASP package [19]. We consider a cubic simulation cell of 64 atoms with periodic boundary conditions, adopting an Fe concentration of $x_{Fe} = 25\%$, with the Fe ions arranged in a regular superlattice with two nearest-neighbor distances between any two neighboring Fe ions (see the Supplemental Material [20]). In order to obtain an efficient simulation setup with well-converged values for internal energy and pressure (within 5 meV/atom and 0.2 GPa), we sample the Brillouin zone at the Baldereschi point [21,22] for a lattice of simple cubic symmetry and use a plane wave cutoff energy of 500 eV. The projector-augmented wave method is used to avoid explicit calculation of the core electron orbitals. To decide on the best feasible approximation to the exchange and correlation part of the total energy functional, we compared the EOS from conjugate-gradient relaxed static calculations

to experiment at 300 K, using the local-density approximation (LDA) and two different generalized-gradient approximations (GGA), PBE [23] and PBEsol [24]. Of these functionals, PBEsol proved clearly superior.

Unfortunately, the PBEsol functional fails to fully capture the strong correlation between the $3d$ electrons of the Fe ions, which is manifested as a spin transition pressure of only 18 GPa for $x_{\mathrm{Fe}} = 3.125\%$, whereas the experimental estimate is closer to 50 GPa [12]. As meta-GGA-type functionals [25–28] that we tested brought no alleviation to this problem, and as hybrid functional calculations utilizing the exact Fock exchange of the DFT system of quasi-electrons are computationally too demanding for MD, we use the $+U$ method [29] to approximate the aforementioned correlation effects. On the basis of our calculations on the dependence of the spin transition pressure on U, an empirical estimate for U from optical spectroscopy data [12], as well as our own hybrid functional [30] computations, we settled on $U - J = 2.5$ eV. We then performed our PBEsol $+ U$ MD simulations in the NVT ensemble using the Nosé-Hoover thermostat. Each simulation was run with a time step of 1.0 fs for a total of 10 ps to reach thermal equilibrium, followed by 10 ps over which all physical time averages were computed. A total of three isotherms, $T = 2000$, 3000, and 4000 K, were simulated for compressions that result in pressures of approximately 0 to 200 GPa, to encompass existing experimental data and the conditions of the lower mantle of Earth. These dynamic computations were complemented with a set of static calculations, where the crystal structure was relaxed using conjugate gradients.

In order to capture the continuous character of the spin crossover and to, thus, produce a first-principles phase diagram of the phenomenon, we minimize the Gibbs free energy $\Delta G(P,T,f) = G(P,T,f) - G(P,T,0)$ at each P and T with respect to f, the fraction of Fe ions in the high-spin state. As we find a vanishingly small amount of intermediate spin ($S = 1$) Fe in our simulations, we define $f \equiv \langle \mu_{\mathrm{Fe}} \rangle / \langle \mu_{\mathrm{Fe}}^{\mathrm{HS}} \rangle$, where μ_{Fe} and $\mu_{\mathrm{Fe}}^{\mathrm{HS}}$ denote the Fe magnetic moment and the same when all Fe ions are in the high-spin state, respectively, and $\langle\rangle$ denotes an average over Fe ions and time. To map $\Delta G(P,T,f) = \Delta H - T\Delta S$ as a function of f, we perform constrained-moment and free-moment calculations, the former producing a low-spin ($f = 0.0$) and high-spin ($f = 1.0$) phase and the latter producing two mixed-spin phases along each isotherm. The enthalpy H of a given phase f is obtained directly from the MD simulation, as is the electronic contribution to the entropy S_{el} [31,32] (we set the electronic temperature equal to the ionic temperature). The vibrational entropy S_{vib} and entropy S_{conf} due to site switching of high spins and low spins we evaluate through the method of thermodynamic integration [33,34]. The last contribution to the entropy, S_{mag}, due to the fully disordered paramagnetic state of the moments above the Néel temperature of ~500 K [35,36], we compute from the expression [37] $S_{\mathrm{mag}} = k_B \sum_i \ln(\mu_i + 1)$, where μ_i is the total magnetic moment of Fe ion i, and k_B is the Boltzmann constant. We thus obtain $\Delta G(P,T,f)$ at four values of f for each P and T, and to find the equilibrium f, we interpolate and minimize $\Delta G(P,T,f)$ with respect to f using a free second-order polynomial (Supplemental Material [20]).

The resulting phase diagram for the spin crossover is presented in Fig. 1. Strikingly, we find a broad pressure interval of coexisting high-spin and low-spin ions at all temperatures, even at fully static conditions ($T = 0$ K in the phase diagram). Another interesting feature of the phase diagram is the weak temperature dependence of the stability field of the mixed-spin phase up to ~3000 K. The shape of our phase diagram is thus fundamentally different from previous theoretical work [10,17,18], where the mixed-spin phase was stabilized through an ideal mixing entropy, resulting in a completely sharp spin transition at $T = 0$ K. We predict $f \approx 0.5$ at the core-mantle boundary, also at odds with previous computations, which have found significantly smaller high-spin fractions. Comparison of our static results to existing experimental EOS, XES, and MSB data at 300 K shows overall good agreement [Figs. 2(a), 2(b)]. Previous computations show a much narrower crossover than EOS, XES, and MSB data and our present results. Despite some experiments indicating a narrow crossover [38], on balance, the crossover would thus appear to be broad rather than narrow, in agreement with our findings. Our results for the EOS at all simulated temperatures are presented in Fig. 2(c), displaying good agreement with experimental high-temperature data.

The finite width of the spin crossover even at vanishing temperatures is due to the favorable enthalpy of mixing ΔH_{mix} of the high-spin and low-spin ions (Fig. 3). We trace the favorable ΔH_{mix} value to packing considerations arising from the volumes of alternating high-spin and low-spin Fe-O octahedra. Because of the occupation of e_g orbitals, the high-spin octahedron is larger than the low-spin octahedron, and the Mg-O octahedron is intermediate in size. When high-spin and low-spin Fe in (Mg,Fe)O are brought close together,

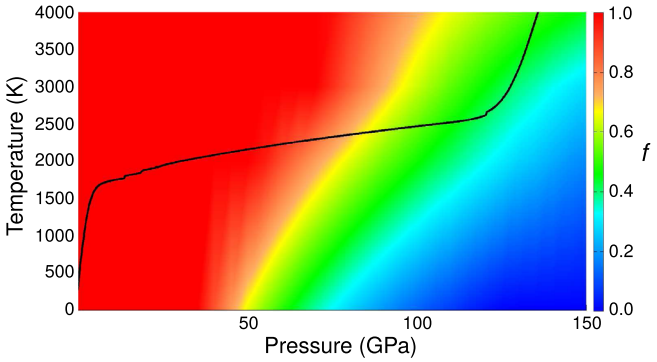

FIG. 1 (color online). Our first-principles phase diagram of the spin crossover in ferropericlase. The black line is a geotherm from Ref. [39].

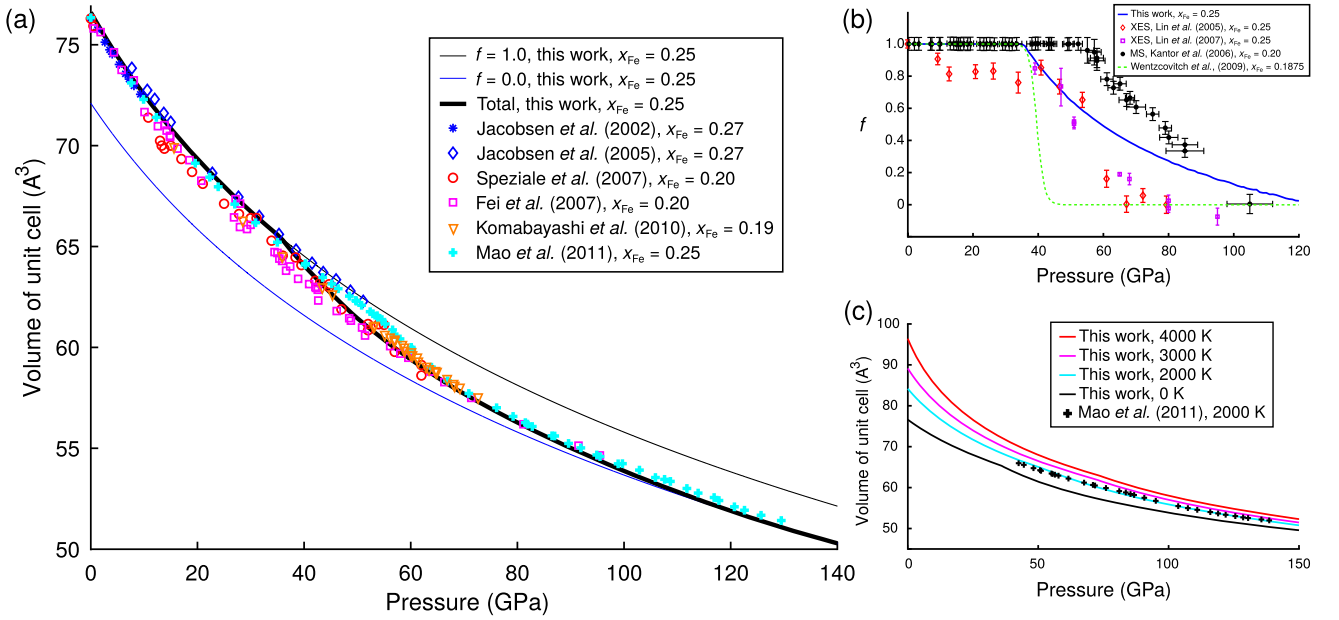

FIG. 2 (color online). (a) The EOS of ferropericlase at static conditions compared to experimental data gathered at 300 K [9,16,40–43]. We construct the total EOS by interpolating $V = V(P, f)$ linearly between the four spin phases f, where the EOS for each phase is a fit to the third-order Birch-Murnaghan EOS [44]. (b) Our static result for f compared to XES and MSB data [8,13,15] as well as previous computational results [10] at 300 K. (c) Our thermal EOS for all simulated temperatures along with experiment at 2000 K [16].

the system can exploit the willingness of high-spin Fe-O octahedra to expand and their neighboring low-spin octahedra to contract with respect to the MgO crystal (see inset of Fig. 3), resulting in lower internal energy and forces and, hence, lower enthalpy than expected from ideal mixing of high-spin and low-spin Fe. Our finding is in sharp contrast to previous computational work on the spin crossover [10,18], where the high-spin and low-spin ions have been assumed to form an ideal solid solution. The favorable ΔH_{mix} value that stabilizes the mixed-spin phase in our static simulations persists in the dynamical simulations (Fig. 3). We quantify the short-range order in our dynamical simulations [20], finding a strongly alternating ordering of high-spin and low-spin octahedra, which is partially relaxed at higher temperature due to vigorous site switching of spins. Finally, while we expect the detailed arrangement of Fe ions in the crystal to affect the magnitude of the mixing enthalpy, the described mechanism stabilizing the mixed-spin phase should not be altered.

Increasing temperature favors the high-spin state because of the favorable contribution to the free energy from the S_{mag} term and to a lesser extent the S_{vib} term. Over the range of temperatures that we have considered, the magnetic entropy dominates over the electronic entropy, which favors the low-spin state. The mixed-spin phase region becomes slightly broader with increasing temperature due to the increase in S_{conf} with increasing temperature. S_{conf} increases with temperature due to the relaxation of short-range order among the Fe sites in the mixed-spin phase (Supplemental Material [20]).

We find that the vibrational entropy is greater for high-spin ions than for low-spin ions. This we relate to the shape of the valence charge density of the Fe ion in the high-spin state which, considering a sole Fe ion in MgO at static conditions and zero pressure, results in a less symmetrical Fe-O octahedron (two axes expanding, one contracting) than that for the low-spin state (all axes contracting uniformly). This underlying differential distortion, as quantified in our NVT simulations by the difference in octahedral quadratic elongation [45] between the high-spin and low-spin phases, persists at finite temperature, leading to larger mean squared displacements of the high-spin Fe ions and, hence, a greater TS_{vib} value in the corresponding phase (Supplemental Material [20]).

The partitioning of Fe between ferropericlase and the major lower mantle phase $(\mathrm{Mg, Fe})\mathrm{SiO_3}$ perovskite has important implications for understanding the structure, dynamics, and geochemistry of Earth's lower mantle [7]. We assess the effect of the spin transition on the partitioning by computing the ratio $\ln(K_f/K_{1.0})$, where K_f is the partition coefficient assuming the equilibrium f, and $K_{1.0}$ is the coefficient assuming $f = 1.0$. Assuming no subsequent spin transition in the perovskite, we find $\ln(K_f/K_{1.0})$ to lie approximately in the range 0 to 1.5 along the geotherm (Supplemental Material [20]), much less than the value of ~10 estimated by Badro *et al.* [7]. Our much more moderate result for the effect of the spin transition on the partitioning appears in better agreement with the relatively weak pressure dependence of K_f found in experiment [1].

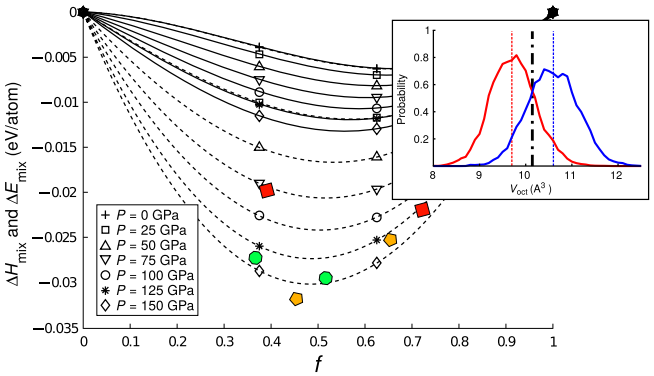

FIG. 3 (color online). Enthalpy (dashed lines) and internal energy (solid lines) of the mixing of high-spin and low-spin Fe at static conditions and the pressures indicated in the legend, along with the enthalpy of mixing at 2000 K and 91 and 64 GPa (green octagons, left to right, respectively), 3000 K and 98 and 73 GPa (orange pentagons), and 4000 K and 106 and 81 GPa (red squares). The lines are fits to $A(1-f)^2f + B(1-f)f^2$. Inset: Distribution of octahedral volumes at 2000 K and lattice constant $\lambda = 3.93$ Å, which yielded $f \approx 0.50$ and $P = 64$ GPa (corresponding to the rightmost green octagon in the main figure), for Fe-O octahedra of high-spin Fe (blue) and low-spin Fe (red). The corresponding static results at the same λ and f are shown by the dashed vertical lines. For comparison, we also show the octahedral volume at static conditions and $\lambda = 3.93$ Å with homogeneous spin states: At the same volume, $f = 1$ and $f = 0$ produce identical values for the Fe-O octahedral volume (to within the thickness of the black dash-dotted line).

The electrical conductivity of the lower mantle is important for understanding anomalies in Earth's rotation via the electromagnetic coupling of mantle and the underlying core and the relationship between observations of the geomagnetic field and its source through the filter of a potentially conductive mantle. However, no measurements or *ab initio* predictions of the conductivity of ferropericlase at conditions of the deep lower mantle are available. Using the Kubo-Greenwood method to compute the electronic component of σ as implemented in VASP [46,47], we find $\sigma = 4.0 \pm 0.4 \times 10^4$ S/m at conditions close to the bottom of the mantle ($P = 136$ GPa, $T = 4000$ K), approximately half the recently obtained value of 9×10^4 S/m for FeO in similar conditions [48], consistent with the experimental result that σ increases with Fe concentration [49]. From the electronic density of states, it is evident that the metallization of the mineral from its initially insulating state is due to the $3d$ electrons of the Fe ions forming broad bands that lead to a significant density of states at the Fermi level, an effect due to both pressure and temperature. The spin crossover itself serves to increase σ, as an increase in the concentration of low-spin Fe implies increased density of states near the Fermi level of the crystal (Supplemental Material [20]).

The predicted semimetallic value of electrical conductivity of ferropericlase at the core-mantle boundary might be invoked to explain the highly conductive layer in this region inferred from observations of the planet's nutations and anomalies therein [50,51]. Assuming the pyrolitic volume fraction of 20% for ferropericlase in the lower mantle, the presently obtained electrical conductivity for the mineral, and taking the surrounding perovskite phase to be insulating, the Hashin-Shtrikman minimum-maximum bounds [52] for the conductivity of the mixture are zero and 5.7×10^3 S/m, respectively. In an adoption of the maximum value and the halfway value, a simple calculation shows that respectively 18 or 35 km of lower-mantle material is enough to give the required minimum conductance of 10^8 S to explain the nutation observations. A more highly conductive mantle than previously assumed may also require revision of the interpretation of surface measurements of Earth's magnetic field.

This research was supported by the European Research Council under Advanced Grant No. 291432 "MoltenEarth" (FP7/2007-2013). Calculations were performed on the Iridis computing cluster partly owned by University College London, and HECToR and ARCHER of the UK national high-performance computing service. The authors acknowledge many valuable comments from R. Jeanloz, as well as fruitful suggestions from R. E. Cohen and B. Militzer.

*e.holmstrom@ucl.ac.uk

[1] J.-F. Lin, S. Speziale, Z. Mao, and H. Marquardt, Rev. Geophys. **51**, 244 (2013).
[2] R. E. Cohen, I. I. Mazin, and D. G. Isaak, Science **275**, 654 (1997).
[3] L. Shulenburger, S. Y. Savrasov, and R. E. Cohen, J. Phys. Conf. Ser. **215**, 012122 (2010).
[4] K. Persson, A. Bengtson, G. Ceder, and D. Morgan, Geophys. Res. Lett. **33**, L16306 (2006).
[5] J. C. Crowhurst, J. M. Brown, A. F. Goncharov, and S. D. Jacobsen, Science **319**, 451 (2008).
[6] M. P. Pasternak, R. D. Taylor, R. Jeanloz, X. Li, J. H. Nguyen, and C. A. McCammon, Phys. Rev. Lett. **79**, 5046 (1997).
[7] J. Badro, G. Fiquet, F. Guyot, J.-P. Rueff, V. V. Struzhkin, G. Vanko, and G. Monaco, Science **300**, 789 (2003).
[8] J.-F. Lin, V. V. Struzhkin, S. D. Jacobsen, M. Y. Hu, P. Chow, J. Kung, H. Liu, H. Mao, and R. J. Hemley, Nature **436**, 377 (2005).
[9] Y. Fei, L. Zhang, A. Corgne, H. Watson, A. Ricolleau, Y. Meng, and V. Prakapenka, Geophys. Res. Lett. **34**, L17307 (2007).
[10] R. M. Wentzcovitch, J. F. Justo, Z. Wu, C. R. S. da Silva, D. A. Yuen, and D. Kohlstedt, Proc. Natl. Acad. Sci. U.S.A. **106**, 8447 (2009).
[11] Z. Wu, J. F. Justo, and R. M. Wentzcovitch, Phys. Rev. Lett. **110**, 228501 (2013).
[12] A. F. Goncharov and V. V. S. S. D. Jacobsen, Science **312**, 1205 (2006).

[13] J.-F. Lin, G. Vanko, S. D. Jacobsen, V. Iota, V. V. Struzhkin, V. B. Prakapenka, A. Kuznetsov, and C.-S. Yoo, Science **317**, 1740 (2007).
[14] A. Bousseksou, G. Molnár, L. Salmon, and W. Nicolazzi, Chem. Soc. Rev. **40**, 3313 (2011).
[15] I. Y. Kantor, L. S. Dubrovinsky, and C. A. McCammon, Phys. Rev. B **73**, 100101(R) (2006).
[16] Z. Mao, J.-F. Lin, J. Liu, and V. B. Prakapenka, Geophys. Res. Lett. **38**, L23308 (2011).
[17] W. Sturhahn, J. M. Jackson, and J.-F. Lin, Geophys. Res. Lett. **32**, L12307 (2005).
[18] T. Tsuchiya, R. M. Wentzcovitch, C. R. S. da Silva, and S. de Gironcoli, Phys. Rev. Lett. **96**, 198501 (2006).
[19] G. Kresse and J. Hafner, Phys. Rev. B **47**, 558 (1993); **49**, 14251 (1994); Phys. Rev. B **54**, 11169 (1996).
[20] See the Supplemental Material at http://link.aps.org/supplemental/10.1103/PhysRevLett.114.117202 for a visualization of the simulation supercell, analysis of the short-range ordering of Fe-O octahedra, details of the free-energy computations, the vibrational entropy results, Fe partitioning, and the electronic band structure.
[21] A. Baldereschi, Phys. Rev. B **7**, 5212 (1973).
[22] R. M. Martin, *Electronic Structure: Basic Theory and Practical Methods* (Cambridge University Press, Cambridge, England, 2008).
[23] J. P. Perdew, K. Burke, and M. Ernzerhof, Phys. Rev. Lett. **77**, 3865 (1996).
[24] J. P. Perdew, A. Ruzsinszky, G. I. Csonka, O. A. Vydrov, G. E. Scuseria, L. A. Constantin, X. Zhou, and K. Burke, Phys. Rev. Lett. **100**, 136406 (2008).
[25] Y. Zhao and D. G. Truhlar, J. Chem. Phys. **125**, 194101 (2006).
[26] J. Tao, J. P. Perdew, V. N. Staroverov, and G. E. Scuseria, Phys. Rev. Lett. **91**, 146401 (2003).
[27] J. P. Perdew, A. Ruzsinszky, G. I. Csonka, L. A. Constantin, and J. Sun, Phys. Rev. Lett. **103**, 026403 (2009).
[28] J. Sun, M. Marsman, G. I. Csonka, A. Ruzsinszky, P. Hao, Y.-S. Kim, G. Kresse, and J. P. Perdew, Phys. Rev. B **84**, 035117 (2011).
[29] S. L. Dudarev, G. A. Botton, S. Y. Savrasov, C. J. Humphreys, and A. P. Sutton, Phys. Rev. B **57**, 1505 (1998).
[30] A. V. Krukau, O. A. Vydrov, A. F. Izmaylov, and G. E. Scuseria, J. Chem. Phys. **125**, 224106 (2006).
[31] N. D. Mermin, Phys. Rev. A **137**, A1441 (1965).
[32] G. Kresse and J. Furthmüller, Comput. Mater. Sci. **6**, 15 (1996).
[33] L. Vocadlo and D. Alfe, Phys. Rev. B **65**, 214105 (2002).
[34] M. J. Gillan, D. Alfe, J. Brodholt, L. Vocadlo, and G. D. Price, Rep. Prog. Phys. **69**, 2365 (2006).
[35] S. Speziale, A. Milner, V. E. Lee, S. M. Clark, M. P. Pasternak, and R. Jeanloz, Proc. Natl. Acad. Sci. U.S.A. **102**, 17918 (2005).
[36] I. S. Lyubutin, V. V. Struzhkin, A. A. Mironovich, A. G. Gavriliuk, P. G. Naumov, J.-F. Lin, S. G. Ovchinnikov, S. Sinogeikin, P. Chow, Y. Xiao *et al.*, Proc. Natl. Acad. Sci. U.S.A. **110**, 7142 (2013).
[37] G. Grimvall, Phys. Rev. B **39**, 12300 (1989).
[38] J.-F. Lin, A. G. Gavriliuk, V. V. Struzhkin, S. D. Jacobsen, W. Sturhahn, M. Y. Hu, P. Chow, and C.-S. Yoo, Phys. Rev. B **73**, 113107 (2006).
[39] L. Stixrude, N. de Koker, N. Sun, M. Mookherjee, and B. B. Karki, Earth Planet. Sci. Lett. **278**, 226 (2009).
[40] S. D. Jacobsen, H.-J. Reichmann, H. A. Spetzler, S. J. Mackwell, J. R. Smyth, R. J. Angel, and C. A. McCammon, J. Geophys. Res. **107**, 2037 (2002).
[41] S. D. Jacobsen, J.-F. Lin, R. J. Angel, G. Shen, V. B. Prakapenka, P. Dera, H. Mao, and R. J. Hemley, J. Synchrotron Radiat. **12**, 577 (2005).
[42] S. Speziale, V. E. Lee, S. M. Clark, J.-F. Lin, M. P. Pasternak, and R. Jeanloz, J. Geophys. Res. **112**, B10212 (2007).
[43] T. Komabayashi, K. Hirose, Y. Nagaya, E. Sugimura, and Y. Ohishi, Earth Planet. Sci. Lett. **297**, 691 (2010).
[44] F. Birch, J. Geophys. Res. **91**, 4949 (1986).
[45] K. Robinson, G. V. Gibbs, and P. H. Ribbe, Science **172**, 567 (1971).
[46] M. P. Desjarlais, J. D. Kress, and L. A. Collins, Phys. Rev. E **66**, 025401(R) (2002).
[47] M. Pozzo, M. P. Desjarlais, and D. Alfe, Phys. Rev. B **84**, 054203 (2011).
[48] K. Ohta, R. E. Cohen, K. Hirose, K. Haule, K. Shimizu, and Y. Ohishi, Phys. Rev. Lett. **108**, 026403 (2012).
[49] X. Li and R. Jeanloz, J. Geophys. Res. **95**, 21609 (1990).
[50] B. A. Buffett, J. Geophys. Res. **97**, 19581 (1992).
[51] B. A. Buffett, E. J. Garnero, and R. Jeanloz, Science **290**, 1338 (2000).
[52] J. G. Berryman, *Rock Physics and Phase Relations: A Handbook of Physical Constants* (American Geophysical Union, Washington, DC, 1995).